Observation of the Structure on Moving Gust Patterns Over a Water Surface ("Cat's Paws")

CRAIG E. DORMAN[1] AND ERIK MOLLO-CHRISTENSEN

Dept. of Meteorology, Massachusetts Institute of Technology, Cambridge 02139

(Manuscript received 3 July 1972, in revised form 6 October 1972)

ABSTRACT

We report on observations of near-surface velocity, temperature, stress, buoyancy, and surface wave fluctuations, including successive short-time averages of coherences, phases, autospectra, and probability densities of the variables. There appear to be short-duration events where the momentum exchange exceeds the average by 10^3. These events are characterized by the high energy content in capillary waves, and velocity and temperature fluctuations; they are separated by relatively quiescent periods. Energy transfer between components is discernible as is a tendency to logarithmico-normal distribution in the occurrence of measures of fluctuations.

1. Introduction

"Cat's paws" is the common name for the ruffles of capillary waves which flit over an otherwise tranquil water surface when first bruised by a zephyr or a breeze. Cat's paws are also observed at higher wind velocities, even in a full gale where moving regions darkened by light refraction in capillary waves appear intermittently, predominantly near the crests of the waves of the dominant sea. The effect of generation of short waves at certain phases of the longer waves may be to mutually enhance the growth rates of both kinds of waves. In order to gain further understanding about these processes, we chose to observe cat's paws in relative isolation, hoping that one would later be able to relate the phenomena of capillary and gravity wave generation as they interact in a rising sea.

The roles of intermittency of generation of waves and turbulence, and of strong nonlinear coupling between scales of motion both within and between the air and water velocity fields, have been largely neglected in the models of wave generation by wind given in the literature (e.g., Jeffreys, 1925, 1926; Phillips, 1957, 1966; Miles, 1957; Hasselmann, 1967, 1971). There is evidence that the presence or absence of capillary waves play a significant role in the process of generation of surface gravity waves. Van Dorn (1953) found that the presence of an oil slick significantly reduced wave generation on an artificial pond, while Ruggles (1969) and Barger *et al.* (1970) found strong effects of an oil slick both in spectra and in wind-wave coherence and phase.

Stewart (1961, 1967) has pointed out that much of the momentum transfer from air to water is effected by wave drag. Van Dorn (1953) and Wu (1969a, 1970) attribute the drag to high-frequency wavelets superimposed on the longer waves. Wu further relates the wavelets to roughness height and states that the momentum flux to wavelets accounts for a substantial portion of the wind stress on the water surface. Longuet-Higgins (1969) has shown that a fluctuating tangential stress occurring selectively near the crests and downwind faces of the longer waves where the shorter waves are trapped (Munk, 1955; Cox, 1958) is dynamically equivalent to a normal pressure fluctuation in quadrature with the sea surface deflection.

The role of turbulence and turbulent Reynolds stress in wave generation has been neglected in much of current theory; Miles (1957) and Phillips (1957) neglect the effect of waves on the turbulent field; Hasselman (1967) includes a weak interaction through disturbances included in the mean flow by one wave component, interaction of this disturbance with a frequency component of turbulence, and a feedback of the resulting pressure disturbance into another wave component.

Intermittent generation of turbulence is a well-known phenomenon in the turbulent boundary layer over a rigid surface; the observations of Kline *et al.* (1967) demonstrate some of the processes involved in such intermittent events. An important element is local instability, the properties of which have been further studied by Landahl (1971).

In a boundary layer over a water surface, local instabilities near the surface will also involve the genera-

[1] Present affiliation: NAVINSWARPAC, U. S. Navy.

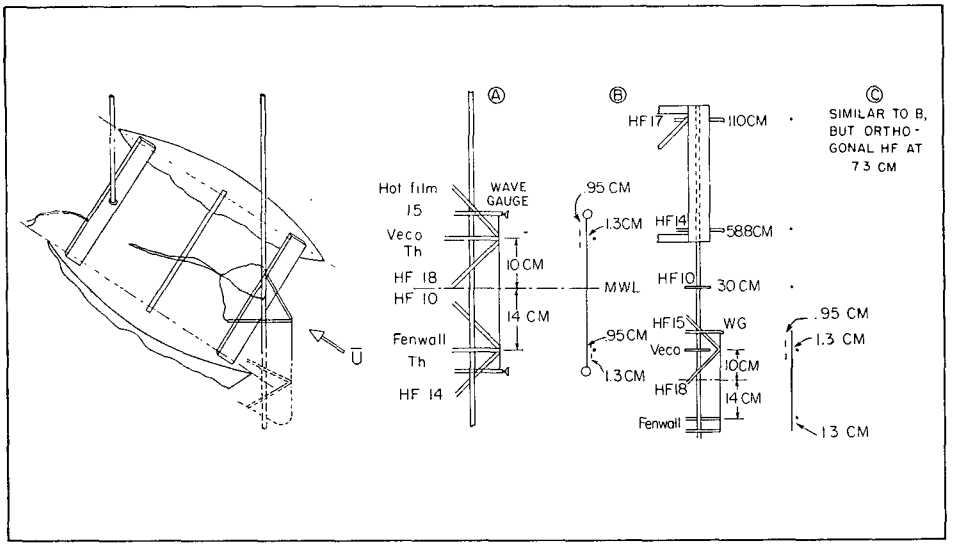

FIG. 1. Sketch of catamaran and instrument configurations (Th, thermistor; HF, hot film anemometer; W.G., wave gage).

tion of waves. A patch of waves will be associated with a patch of Reynolds stress involving fluctuations of the same wavenumber and frequency as the waves. The patch of waves being generated then appears to the oncoming flow as a high stress zone and the scale of the pressure fluctuation will be the scale of the patch, rather than only the scale of the waves in the patch. This can be seen by taking the divergence of the momentum equation for inviscid, incompressible flow, yielding

$$\nabla^2 p = -\partial^2(\rho u_i u_j)/\partial x_i \partial x_j. \qquad (1.1)$$

Since $u_i u_j$ has a non-zero average over a wavelength of the disturbance being generated, these averages add up over the patch to give an overall stress and pressure field with the scale of the patch. Such a pressure field will generate waves of wavelength comparable to the scale of the patch; the occurrence of longer waves may then enhance the velocity anomaly which led to local instability in the first place and lock the phenomena of short- and long-wave generation together for awhile.

The actual processes seem to be more complicated than the single nonlinear coupling sketched above, in the sense that many scales seem to interact simultaneously and in sequence during a generation event. Our present results serve to demonstrate some of these processes, even though the resulting illumination is far from complete.

2. Experiment arrangement

The sensors were mounted on a 1 m long surface following a catamaran (Fig. 1). The catamaran was

TABLE 1. Catamaran runs (2-hr duration).

Run no.	Instrument configurations	U (m sec^{-1})	T_{air} (°C)	T at H_2O (°C)	$Ri=\frac{2(\theta_a-\theta_w)}{U^2/a}$	Mean waves: Period (sec)	Mean waves: Height (inches)	Comments
2	A+	W,6–8	5.0	4.12	0.05	1.3–1.7,	4–6	Gusting to 12 m sec^{-1}, many cat's paws and active generation; sea nearly fully developed.
3A	A+	W,2	6.7	4.20	1.25	calm		Low wind, few gusts.
3B	A+	W,0–5	7.2	4.22	0.75	calm–1,	0.5	Two periods of slow wind increase to 5 m sec^{-1}, then return to calm.
4	A	E/W,3–5	11.9	5.0	0.85	start: 1.2, end: 1,	5–6 2	Generally dying winds, gusty near start. Some segments in natural slick.
5	B	W,4–5	9.2	5.4	0.31	1.35,	4–5	Occasional gusts to 8 m sec^{-1}; large T fluctuations from cloud passage; some slicks.
6A	B	E/W,0–1	9.4	5.8	7.2	calm		Sunny, light and variable winds with occasional gusts.
6B	C	E/W,0–1	11.2	6.9	8.6	calm		Same as 6A.

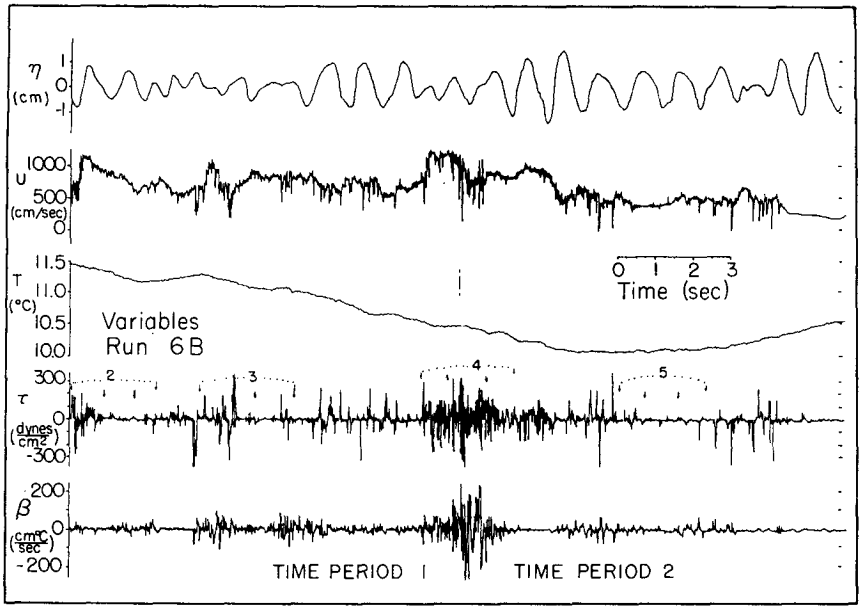

FIG. 2. Wave signal (η), horizontal air speed (U), air temperature (T), Reynolds stress ($\tau = -\rho u'w'$), and buoyancy fluctuations ($\beta = T'w'$) for the first and second 10-sec periods of Run 6B.

free in roll, heave and pitch, and restrained in yaw and horizontal translation. It could be oriented into the wind. The experiment was conducted in March 1971 from the dock of the M. I. T. Nautical Association on the Charles River Basin, Cambridge, Mass.

The catamaran had two masts sliding in sleeve bearings in an overhead structure; the masts were gimbal-mounted on the catamaran. All sensors were mounted on the forward mast, so the instruments moved along a fixed vertical line with the heave of the mast step gimbal of the catamaran. The instruments included six Disa type 55A81 hot film anemometers, a capacitance wave sensor of diameter 0.076 cm, a Veco 42A70 thermistor in the air, and a Fenwall K496 thermistor in the water. Subsidiary instrumentation included an accelerometer for sensing catamaran motion and cup and propeller anemometers for determining mean wind speed. The data were recorded on magnetic tape and accompanied by voice narration that was later used for subjective conditional sampling of the signals.

Two of the hot film anemometers were orthogonally mounted to give horizontal and vertical velocities (u, w). Table 1 lists the instrumental arrangements and mean conditions for the seven 2-hr runs that were analyzed. Data from Runs 2, 4 and 6B, which represent the full range of conditions encountered, were selected for inclusion in this paper.

The data were analyzed using a combination of digital and analog processing. Pre-analysis, demodulation and filtering (100-Hz low pass) were done by analog methods. The data were then digitized at a sampling rate of 250 Hz and recorded on seven track digital tape, preparatory to processing on the M. I. T. IBM-360 computer system. Extensive use was made of graphical computer output from a Stromberg-Carlson 4020 plotter.

The major difficulty in the data interpretation was caused by the motion of the catamaran. Its heave resonance frequency was approximately 1.5 Hz; it therefore did follow the low-frequency waves whose spectral growth, for example, could not be calculated.

3. Results

a. Variables as functions of time

Figs. 2 and 3 show four successive 10-sec periods during a cat's paw passage (Run 6B). The variables are wave gage output η and air velocity U at $z = 10$ cm, air temperature (T), stress ($-\rho u'w' = \tau$), and "buoyancy" ($\beta = w'T'$) at $z = 7.3$ cm. The fluctuations u', w', and T are defined as the departure from the average in each 10-sec time period. Thus, different 10-sec time periods will have different average values. Additionally, there were slight intervals of time between 10-sec periods, since it was difficult to join successive files of samples closely. Each 10-sec period contains 2520 samples of each of the variables.

Before we discuss Figs. 2 and 3, we show similar results for two more cat's paws; Runs 2 and 4, in Figs. 4–6. For Run 4 (Fig. 6), a measure of intermittency is shown, namely a variable which is zero when $\tau < 100$ dyn cm^{-2} and unity otherwise. Fig. 6 also shows the water temperature and the water momentum transport $-\rho_w u_w' w_w' = \tau_w$, both at $z = -13$ cm.

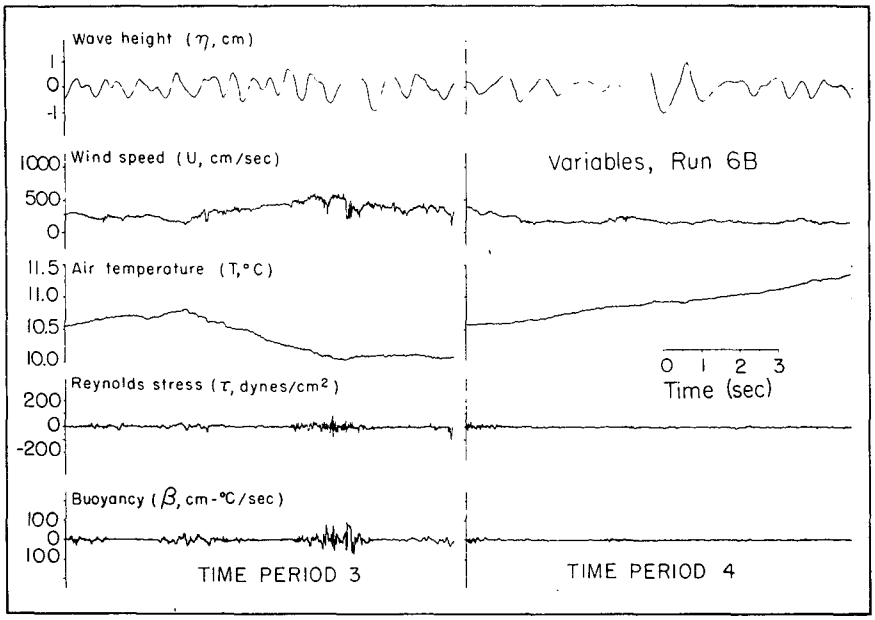

FIG. 3. Same variables as Fig. 2 for the third and fourth 10-sec periods of Run 6B.

These results show that a cat's paw is associated with a gust (we caught it a little late in Fig. 2). The wind increases locally with time, the air temperature drops, and the turbulent momentum flux oscillates wildly with values of several hundred times the average flux. The intensive exchange of heat and momentum then dies down to the typical average picture which is similar to the last 10-sec period shown in Fig. 3, with an average Reynolds stress of 0.5 dyn cm^{-2}. Fig. 6 indicates that the water momentum exchange comes later than the high stress in the air.

To further emphasize the difference between maximum and minimum activity, Fig. 7 shows 2-sec segments of Run 6B, namely the first 2 sec of the second and fourth 10-sec periods. In this figure, use has been made of the self-scaling routine of the computer graphics program, which divides the ordinate of a variable by its maximum and writes the maximum

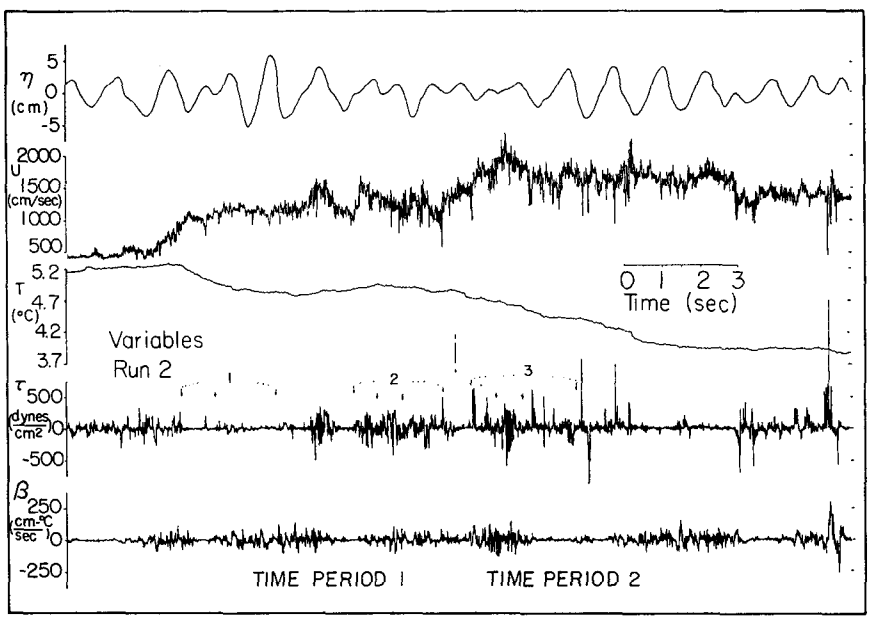

FIG. 4. Same as Fig. 2 for Run 2.

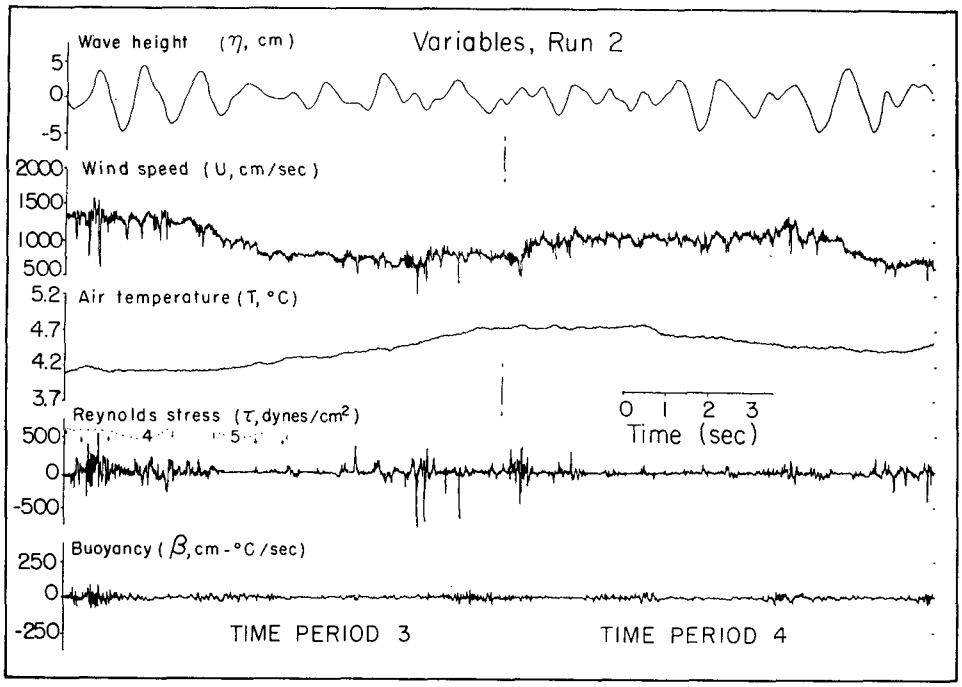

FIG. 5. Same as Fig. 3 for Run 2.

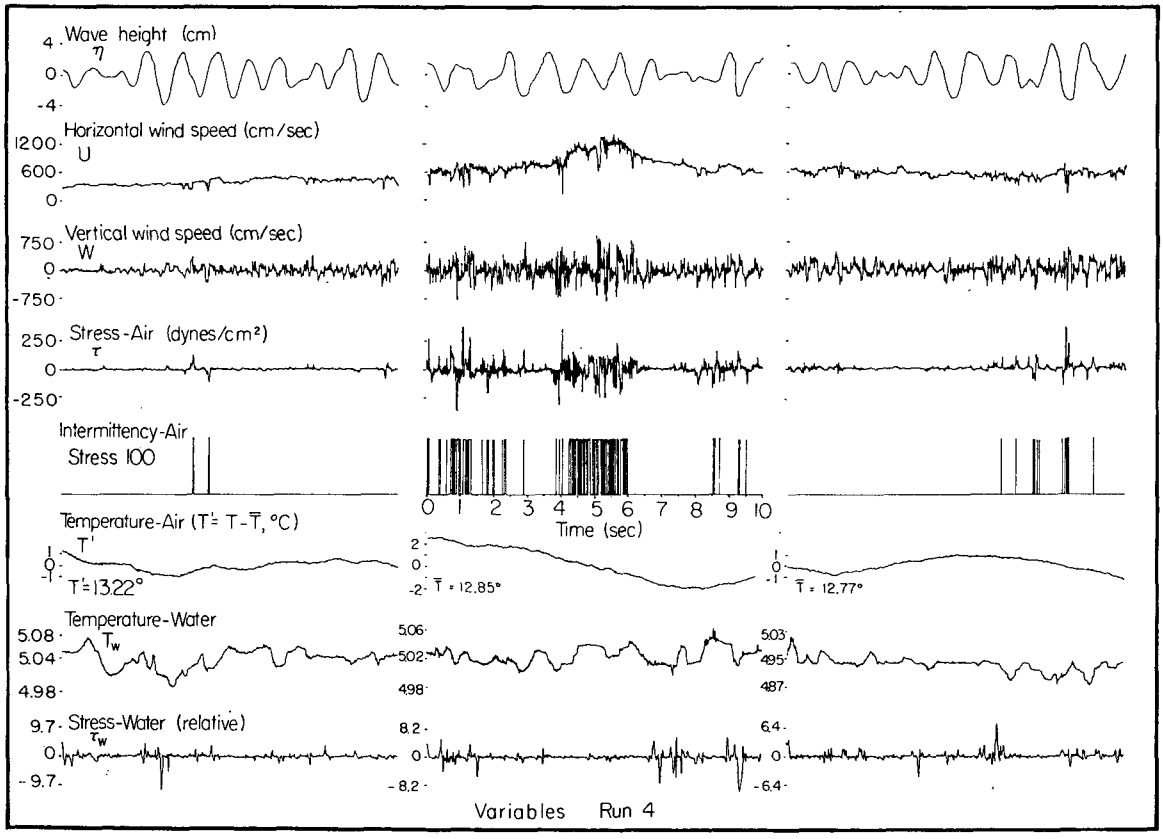

FIG. 6. Data from three 10-sec periods of Run 4. The intermittency trace shown is unity when the Reynolds stress in the air exceed 100 dyn cm^{-2}, zero otherwise.

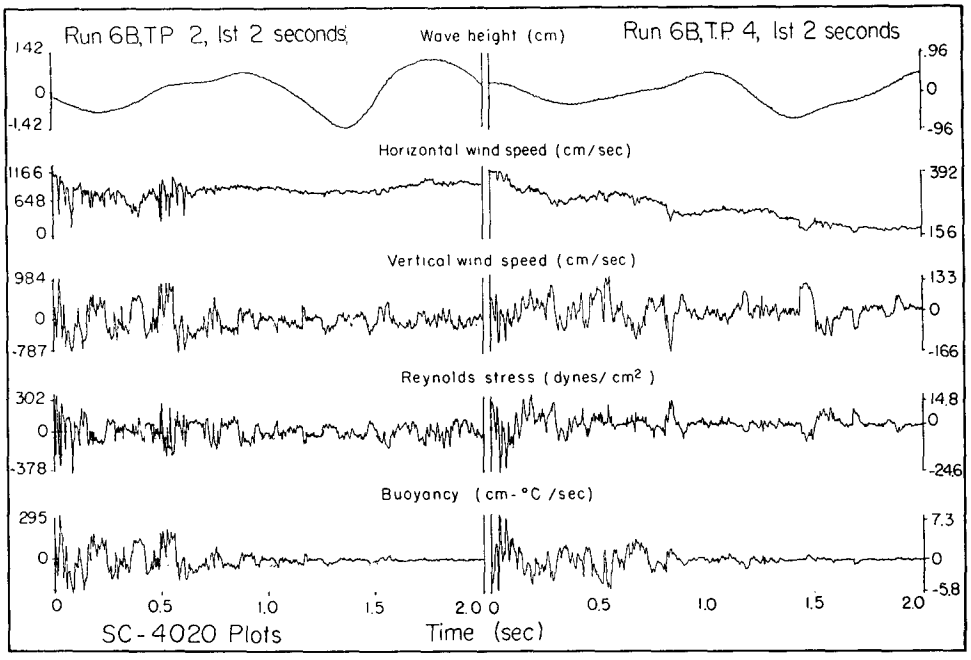

FIG. 7. Traces from two selected 2-sec periods of Run 6B (note change in vertical scales in the two time segments).

value on the ordinate. Thus, the stresses have maxima of 302 and 14.8 dyn cm^{-2}, respectively, in the two 2-sec intervals.

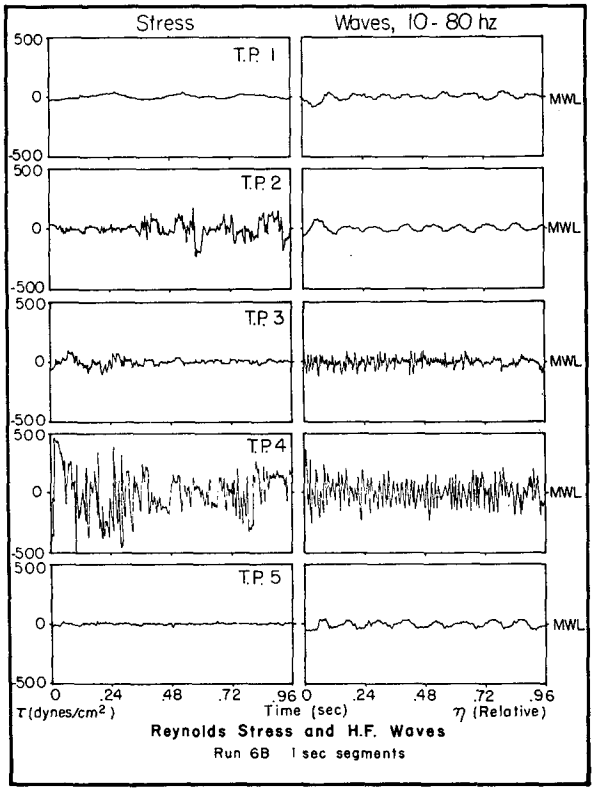

FIG. 8. Instantaneous Reynolds stress and band-pass filtered wave gage output in corresponding 1-sec periods.

Fig. 8, also from Run 6B, shows τ and a filtered wave signal in five selected 1-sec segments (indicated in Fig. 2 with the exception of the first segment which is from before gust arrival). The occurrence of strong τ fluctuations is seen to coincide with high capillary wave energy in the frequency range of 10–80 Hz. This suggests that turbulence generation, high stress, and generation of capillaries may be joint events. Fig. 9 shows profiles of normalized (to 10-sec mean) hot-film outputs averaged over 0.5-sec periods to indicate horizontal velocity fluctuations. Also shown are running second averages of four-point (z-average) wind velocity $\bar{U}_{0.5s}$ and turbulence production as

$$P = -\langle u'w' \rangle_{0.5s} \frac{\bar{U}_{0.5s}}{z},$$

where

$$\bar{U}_{0.5s} = \tfrac{1}{4} \sum_{j=1}^{5} \langle U(t,z_j) \rangle_{0.5\ \mathrm{sec}},$$

$\langle\ \rangle_{0.5s}$ being a 0.5-sec time average operator and z the height of the $u'w'$ probes.

Outputs from the bottom two hot-films were used to compute the gradient.

One can only say that production seems to coincide with large fluctuations in velocity profile, that production is intermittent, and that the last 10-sec calm period is very calm indeed. The large profile anomalies coincide with the strong bursts or stress fluctuations shown in Figs. 2 and 3.

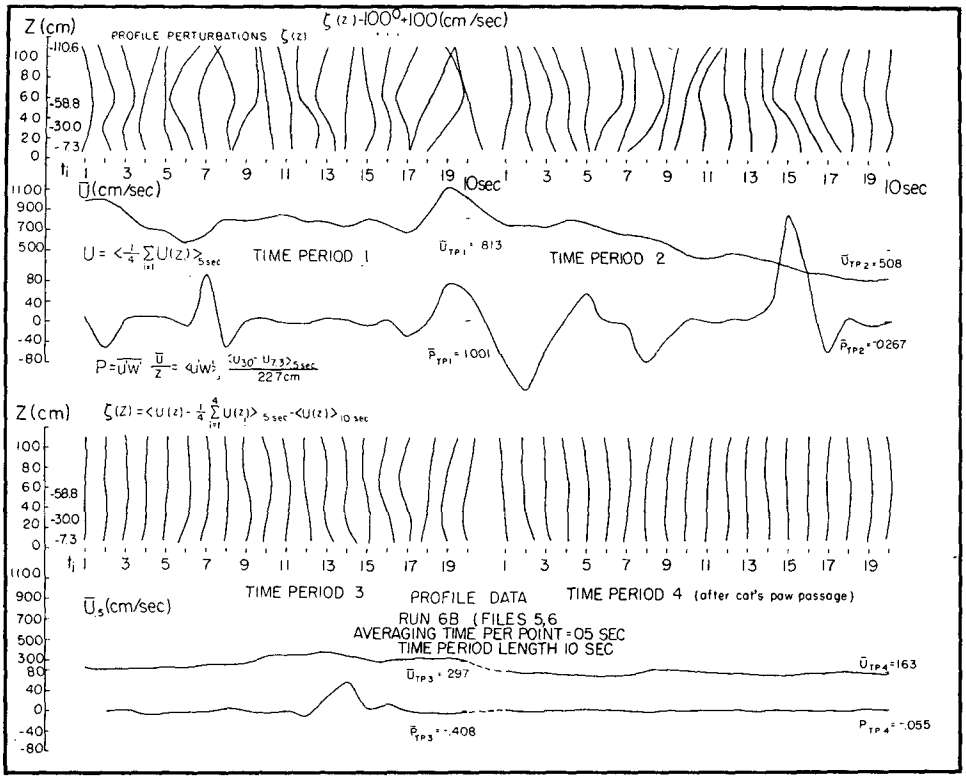

FIG. 9. Perturbation velocity profiles, horizontal velocity, and turbulence production: $P=u'w'(\bar{U}/Z)$ average of $\frac{1}{2}$ sec for Run 6B.

b. Short-time average measures

When one samples fluctuations conditionally, by selecting events as we have done, one must use caution in the interpretation of statistical measures. When dealing with highly intermittent processes, where significant activity occupies a small time fraction, the activity will be diluted by averages over times when nothing happens. When dealing with events with a characteristic infrastructure, long time averages may be misleading in the sense that the average does not represent a physical process which actually occurs, but rather the average of even opposite processes.

The alternative to time averaging is ensemble averaging. If all cat's paws were alike in sequence of events and duration, one could take a large number of them and superimpose their characteristics to arrive at a description of an "average" cat's paw. Cat's paws do seem to differ in duration and character; to find scaling rules which would enable us to superimpose them will not be easy. We have therefore compromised and used the measures usually applied to stationary processes to average over finite time intervals.

Since some of the variables have non-Gaussian distributions, and are non-stationary over the averaging times used, no conclusions can be drawn about significance or error margins. Nevertheless, finite-time average measures still reveal characteristics of a process which may be helpful for description, and which may suggest the criteria or algorithms to be used for automatic conditional sampling.

We hope that the reader will not be offended by our use of the standard terminology for measures and joint measures customarily applied to stationary random processes for the finite-time average measures we present here.

c. Power spectral densities

Fig. 10 shows 10-sec average spectral densities for Run 6B. The spectral density of u' drops by over 10^2 between 10-sec time periods 2 and 4, likewise for the spectral densities of w, τ and wT. Fig. 11 shows wave spectra from Run 6B with 2-sec time averaging. There are no large changes in wave spectra except for the occurrence of a decrease of between one and two orders of magnitude in the energy content between 10 and 11 Hz. One may take this as an indication that after the waves have been generated they are subject to nonlinear interaction of the kind first noted by Wilton (1915) and analyzed by McGoldrick (1965), which predicts that self-resonant interaction occurs for a certain wave frequency near where capillarity and gravity are equally important in their effect on wave dispersion.

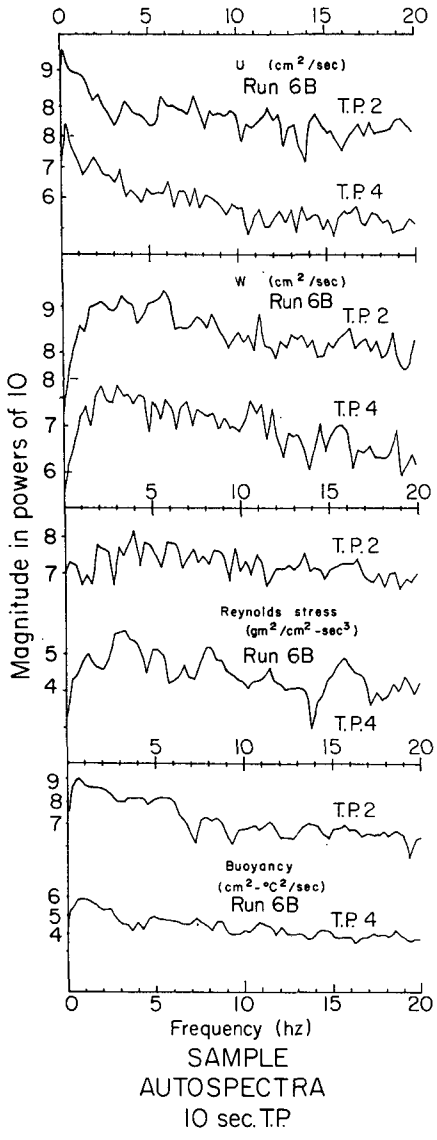

FIG. 10. Power spectral densities of horizontal velocity U, vertical velocity W, Reynolds stress $-\rho u'w'$, and buoyancy $w'T'$ for the second and fourth 10-sec time periods of Run 6B.

d. Joint histograms

Joint histograms show the occupation density in the sample space of joint events.

For example, Fig. 12 shows joint histograms of $\tau = -\rho u'w'$ and $\beta = w'T'$ in the four 10-sec time periods of Run 6B. These histograms are included to show that a 10-sec sample only shows weak correlations, in contrast with shorter samples. One may interpret this to mean that a 10-sec time period includes several different phenomena, each with a different joint distribution function.

It seems as if there may first be a tendency for positive correlation between β and τ, then negative then again positive. The negative correlation, if indeed present, may be caused by the local velocity field responding to the high surface Reynolds stress associated with generation of turbulence, which tumbles an air parcel upside down, thus inverting the local vertical temperature gradient. The figure also shows the time traces of 10-sec average values of u, T, τ and β.

Similarly, a corresponding set of β-τ histograms from Run 2 (Fig. 13) seems to mix up several smaller events, not as clearly separated so that TP1 and TP2 contain both positively and negatively correlated events. This is supported by Fig. 14, which shows histograms from Run 2 for the 2-sec time periods indicated in Figs. 4 and 5. Positively and negatively correlated patterns now show up separately.

A set of joint histograms of u and T taken over 10-sec periods of Run 6B (at $z = 7.3$ cm) are shown in Fig. 15. The first histogram shows the bimodal temperature distribution; the second, bimodal velocity and temperature fluctuations. The amplitude of temperature fluctuations lags the large-amplitude velocity fluctuations and persists longer. It seems that the stress associated with generation of turbulence makes the temperature field tumble, and the thermal stratification is then restored by gravity. It also appears that there are couplings of different phase relation between the thermal and the velocity fields. These are seen when one

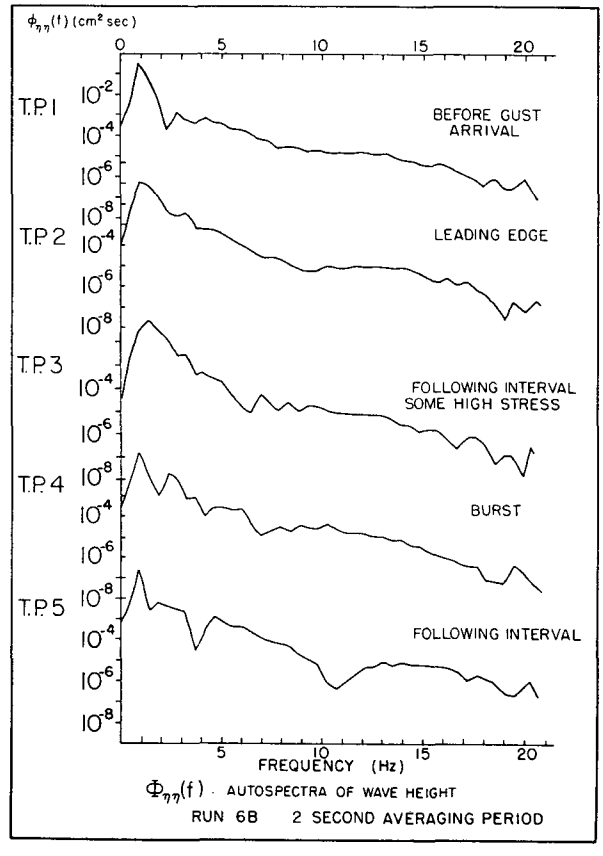

FIG. 11. Power spectra of water surface deflection (wave spectra for successive time periods of a cat's paw passage.

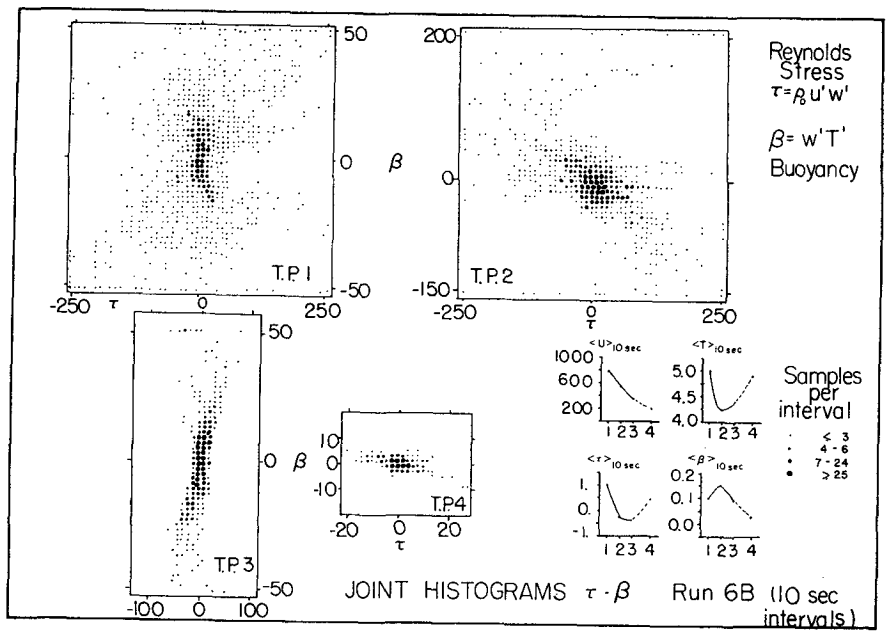

FIG. 12. Joint histograms of instantaneous stress $\tau=-\rho u'w'$ and buoyancy $\beta=w'T'$ for successive 10-sec periods for Run 6B.

examines the coherence and phase of variables associated with the two fields.

e. Cross-spectral information

Define the coherence $\mathrm{Coh}(\omega)$ and phase $\theta(\omega)$ spectra of two variables $a(t)$ and $b(t)$ as the magnitude and phase of the cross-spectral density $\phi_{ab}(\omega)$, where

$$[\overline{a^2}\ \overline{b^2}]^{\frac{1}{2}}\phi_{ab}(\omega)=\int_{-\infty}^{+\infty}\overline{a(t)b(t+\tau)}e^{i\omega\tau}d\tau,$$

$$\phi_{ab}(\omega)=\mathrm{Coh}(\omega)e^{i\theta(\omega)}$$

$$=C(\omega)+iQ(\omega),$$

$C(\omega)$ is the cross spectrum, $C(\omega)=\mathrm{Coh}(\omega)\cos\theta(\omega)$; $Q(\omega)$ is the quadrature spectrum, while $\overline{a(t)b(t+\tau)}$ is the cross correlation between $a(t)$ and $b(t+\tau)$, a function of delay time τ. $\mathrm{Coh}(\omega)$ describes the amplitude correlation between the same frequency component of the two signals; $\theta(\omega)$ describes their relative phase.

One can perform the same operations on averages of $a(t)b(t+\tau)$ over finite-time intervals, and determine $\mathrm{Coh}(\omega)$ and $\theta(\omega)$ for such finite-time samples. For example, for surface waves undulating a thermally stable air layer, the coherence between air temperature and waves should be high and the phase near $\pm\pi$, since

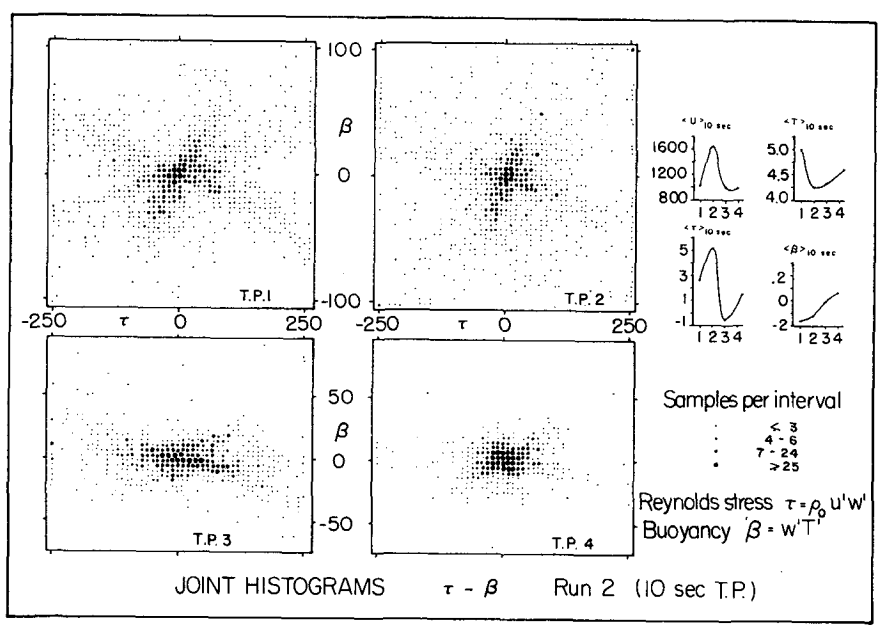

FIG. 13. Same as Fig. 12 for Run 2.

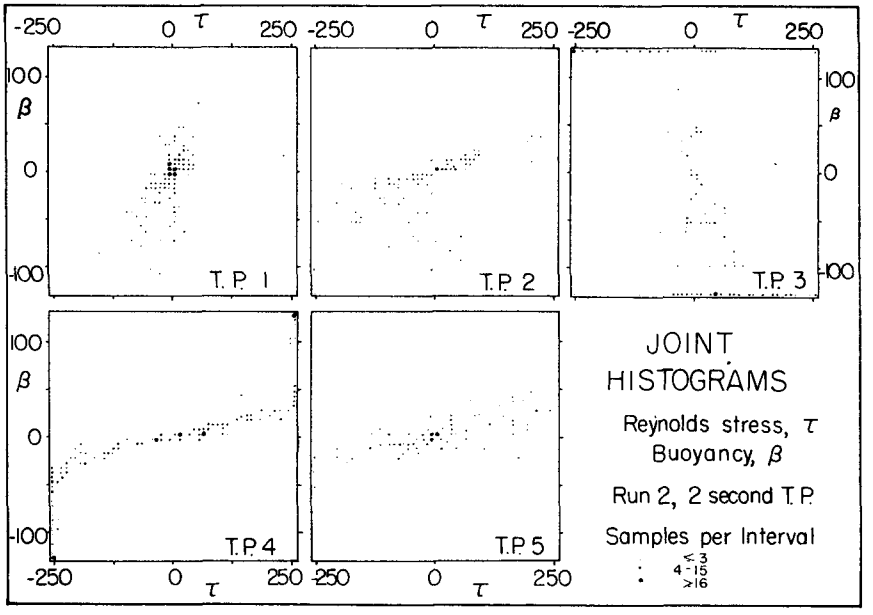

FIG. 14. Joint histograms of Reynolds stress τ and buoyancy β for 2-sec time periods (Run 2).

colder air is lifted by the wave crest. Fig. 16 shows this for 10-sec periods from Run 4. The coherence is high with phase angles near π at first. The phase angle decreases during the next time interval and is small in the last period. The peculiar behavior of both coherence and phase near a frequency of 15 Hz may be real, since it is near the boundary between capillary and gravity waves. Fig. 16 also shows the coherence of stress and buoyancy for Run 4. Again, while the coherence is low, the phase definitely is either near zero or near π also showing the reversal of buoyancy.

This is even more striking when one looks at shorter time periods where short-duration important events can be segegrated. Fig. 17 shows stress-buoyancy coherence and phase for five selected 1-sec intervals in Run 6B (the same periods as shown in Fig. 8). The coherence and phase are 1 and 0 at first, probably indicating that prior to gust arrival all the turbulence is in the form of internal gravity waves or stability fluctuations. Then the phase becomes π, indicating a reversal of the temperature stratification, probably due to tumbling of air parcels due to high surface stress

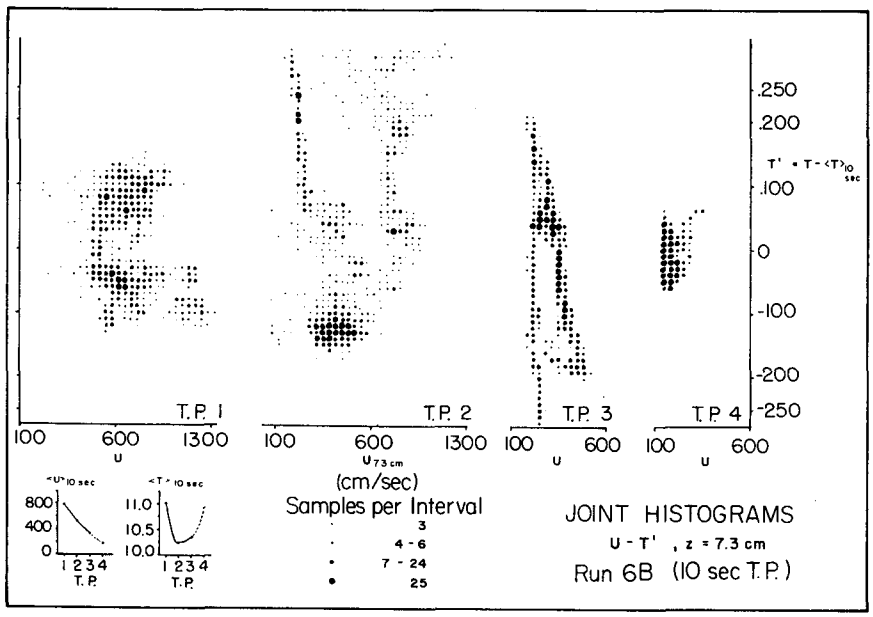

FIG. 15. Joint histograms of U and T' for 10-sec time periods (Run 6B).

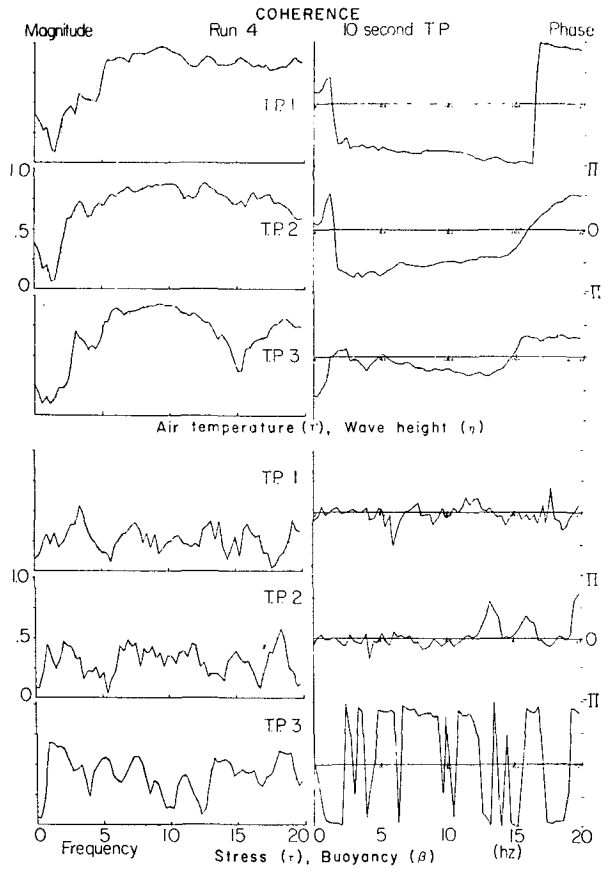

FIG. 16. Coherence (left) and phase (right) of air temperature and wave height, and of stress τ and buoyancy β averaged over 10-sec time periods.

(TP2 and TP3). It should be remarked that this overturning of air parcels may be caused by streamwise as well as cross-stream vorticity, as suggested by the observations of turbulent spots by Kline *et al.* (1967).

This strong tendency for 0 or π phase angles indicated that this phenomenon is highly structured.

f. Probability densities of variables

Calculating short-time probability densities of a variable is not significant in the conventional sense because of the limited samples. As with frequency domain measures, however, one may discern features not at first obvious from time records that are of importance in identifying significant processes. In this paper, we only show a measure of turbulence which should have an approximately log-normal distribution function according to the hypothesis of Gurvich and Yaglom (1967). The measure selected is the normalized square time derivative of the horizontal velocity, smoothed over five successive samples as suggested by Chen and defined by:

$$\psi=\ln\Big[\tfrac{1}{5}\sum_{j=1}^{5}\xi(t-j\Delta t)\Big],$$

where

$$\xi(t)=\left(\frac{\partial u}{\partial t}\right)^2\Big/\overline{\left(\frac{\partial u}{\partial t}\right)^2}.$$

The probability function of this measure is plotted on normal probability paper in Fig. 18 for selected 2- and 1-sec time periods for Runs 2 and 6B. A log-normal distribution of ξ will give a straight line on the diagram. The straight lines corresponding to log-normal distributions with the observed mean and variance are shown. The mean is denoted by a tick mark on each distribution curve. For Run 2, the mean, variance, skewness and kurtosis are tabulated in Table 2.

The results show that 2-sec time averages fit log-normal better than 1-sec averages, that there are especially significant departures from the mean at large and small values, and that the variance is larger in what we subjectively have classified as "bursts" by looking at the time records.

The observed kurtosis in the distribution of ξ, which is of order 10^3, indicates that the likelihood of large departures from the mean is very high, the contribution may come from a few exceptional events, and the number of such events may change wildly from sampling period to sampling period. The statistical significance

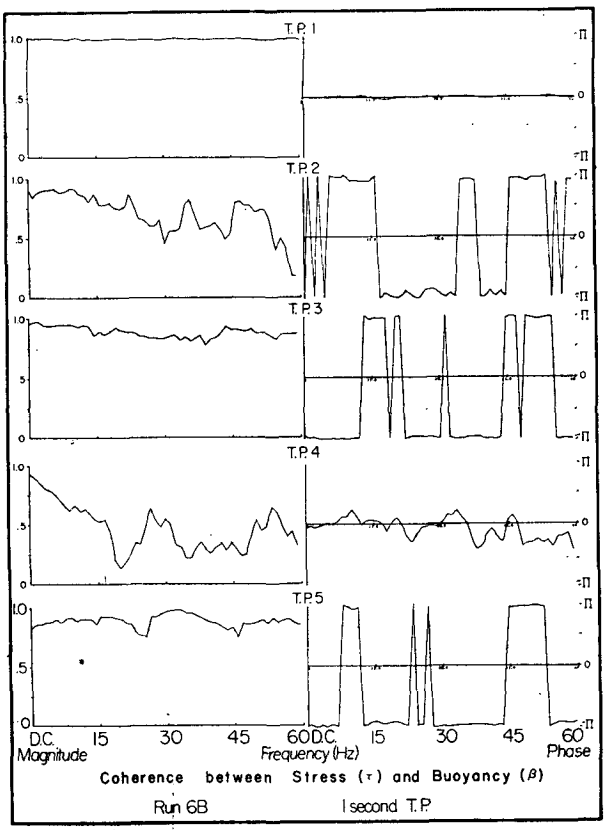

FIG. 17. Coherency between stress τ and buoyancy β averaged over 1-sec time intervals.

of the results is therefore tenuous at the extremes of the curves.

According to Gurvich and Yaglom, samples over a given time scale should give the same distribution function. Our data may include insufficient samples to justify a conclusion about this. However, if the distribution functions for different time intervals of the same length were perfectly log-normal, but with different dispersions, the sum of the distribution functions would not be log-normal.

This suggests the possibility, physically rather likely in this particular experiment, that the anisotropy of the bursts will affect the distribution function. This means that in the phenomena we are observing, a single-length scale may be insufficient for describing the turbulent breakdown regions and that several-length scales, their ratio varying with the class or age of the burst, need to be considered. This does not by itself invalidate the hypothesis of Gurvich and Yaglom as applied to homogeneous turbulence. The results suggest, however, that the physics of breakdown even in homogeneous turbulence may involve anisotropic imbedding of bursts within bursts, and thus require more than one length scale to describe the orientation of elongated or flat regions of bursts within larger scale bursts.

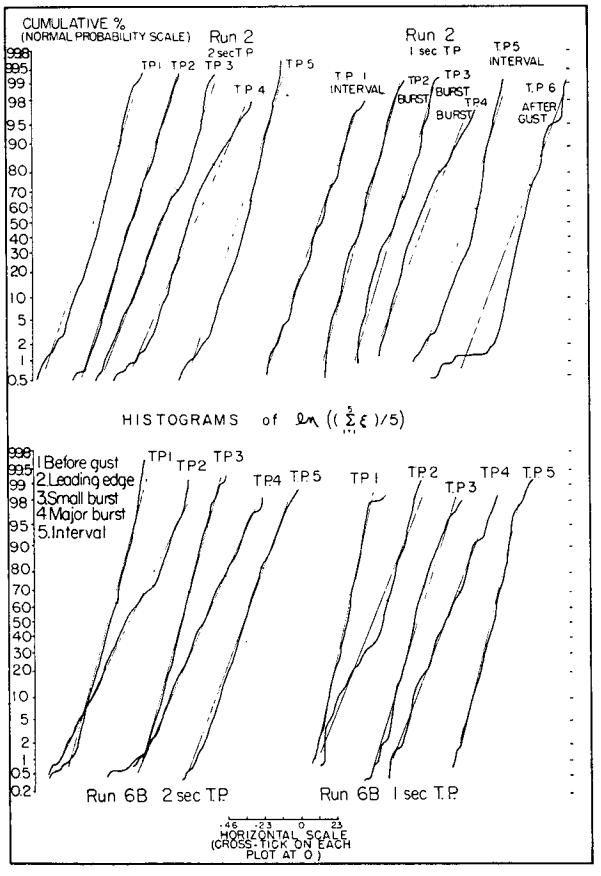

FIG. 18. Histograms (probability density) of the natural logarithm of short-term averages of $(\partial u/\partial t)^2$ plotted on normal probability paper for 2- and 1-sec time periods of Runs 2 and 6B.

TABLE 2. Statistical properties of $\xi=\frac{1}{5}\sum_{j=1}^{5}\left[\left(\frac{\partial u}{\partial t}\right)^2_{t_j}\Big/\left(\overline{\frac{\partial u}{\partial t}}\right)^2\right]$ in five 2-sec time periods in Run 2. $t_j-t_{j-1}=\Delta t=1/2023$ sec.

Time period	Mean	Variance	Skewness	Kurtosis
1	−0.59	3.01	−42.07	942
2	−0.26	3.16	−40.35	916
3	−1.11	4.04	−38.34	866
4	−1.56	3.95	−33.83	806
5	−0.54	2.99	−42.55	951

4. Conclusions

These observations represent an attempt to describe the processes involved in the generation of turbulence and waves, and the transport of momentum and heat in a gust over a water surface. The data indicate that turbulence generation, wave generation, and the occurrence of large fluxes are conjoint events occurring intermittently, occupying less than 5% of the total time or area while accounting for most of the average transport.

The turbulent stress field near the water surface associated with capillary wave generation will make the temperature field in the air tumble; the scale of this tumbling is much larger than the wavelengths of capillary waves. There is some evidence for nonlinear wave interaction of the type described by Wilton (1915), removing energy from the wave spectrum near the frequency of minimum celerity near 10 Hz.

The tendency toward log-normal distributions of ψ supports the hypothesis of Gurvich and Yaglom (1967). The variation in dispersion needs to be explored further.

Surface stress is intermittent. The average surface stress is mainly supported by intermittent bursts occurring in conjunction with capillary wave generation. We further suggest that in the generation of large sea surface waves, these bursts of generation occur preferentially at some phases of the large-scale wave field, playing an important role in the wave generation process.

The observed intermittency of the stress field indicates that observation of long time averages will not reveal the physics of air-sea interaction unless one directly measures variables characteristic of bursts, such as turbulent stress, heat transfer, and capillary wave energy. Our observations suggest that the coupling between scales of motion of millimeters and many meters plays an important role in wave and turbulence generation, the small scales acting as catalysts for extraction of energy by the large-scale fluctuations from the mean field.

In order to identify and classify these interactions, more observations are indicated, preferably at Reynolds numbers beyond those attainable in small-scale lab-

oratory experiments. Such observations will always suffer from the shortcomings of those reported here, namely a lack of control of external parameters subject to the vagaries of nature.

Acknowledgments. The research reported on here was supported by the Office of Naval Research under Contract NR 083-236, and by the National Science Foundation under Grant GA 28622X.

REFERENCES

Barger, W. R., W. D. Garrett, E. L. Mollo-Christensen and K. W. Ruggles, 1970: Effects of an artificial sea slick upon the atmosphere and the ocean. *J. Appl. Meteor.*, **9**, 396–400.

Cox, C. S., 1958: Measurements of slopes of high-frequency waves. *J. Marine Res.*, **16**, 199–225.

Gurvich, A. S., and A. M. Yaglom, 1967: *Phys. Fluids Suppl.*, **10**, S59–S65.

Hasselmann, K., 1967: Non-linear interactions treated by the methods of theoretical physics. *Proc. Roy. Soc. London*, **A299**, 77–100.

——, 1971: On the mass and momentum transfer between short gravity waves and larger scale motions. *J. Fluid Mech.*, **50**, 189–205.

Jeffreys, H., 1924: On the formation of water waves by wind. *Proc. Roy. Soc. London*, **A107**, 189–206; 1925: **A110**, 341–347.

Kline, S. T., W. C. Reynolds, F. C. Schraub and P. W. Runstadler, 1967: The structure of turbulent boundary layers. *J. Fluid Mech.*, **30**, 741–773.

Landahl, M. T., 1972: Wave mechanics of a breakdown. *J. Fluid Mech.* (to be published).

Longuet-Higgins, M. S., 1969: On the action of a variable stress at the surface of water waves. *Phys. Fluids*, **12**, 737–740.

McGoldrick, L. F., 1965: Resonant interaction among capillary-gravity waves. *J. Fluid Mech.*, **21**, 305–331.

Miles, J. W., 1957: On the generation of surface waves by shear flows. *J. Fluid Mech.*, **3**, 185–204.

Munk, W., 1955: High frequency spectrum of ocean waves. *J. Marine Res.*, **14**, 302–314.

Obukhov, A. M., 1962: Some specific features of atmospheric turbulence, *J. Fluid Mech.*, **13**, 77–81.

Phillips, O. M., 1957: On the generation of waves by turbulent wind. *J. Fluid Mech.*, **2**, 417–445.

——, 1966: *The Dynamics of the Upper Ocean.* Cambridge University Press, 259 pp.

Ruggles, K. W., 1970: The vertical mean wind profile over the ocean for light to moderate winds. *J. Appl. Meteor.*, **9**, 468–474.

Stewart, R. W., 1961: The wave drag of wind over water. *J. Fluid Mech.*, **10**, 189–194.

——, 1967: Mechanics of the air-sea interface. *Phys. Fluids Suppl.*, **10**, S47–S65.

Van Dorn, W., 1953: Wind stress on an artificial pond. *J. Marine Res.*, **12**, 249–276.

Wilton, J. R., 1915: On ripples. *Phil. Mag.*, **29**, 688–700.

Wu, J., 1969a: A criterion for determining air-flow separation from wind waves. *Tellus*, **21**, 707–713.

——, 1969b: Wind stress and surface roughness. *J. Geophys. Res.*, **74**, 444–455.

——, 1970: Wind-wave interactions. *Phys. Fluids*, **13**, 1926–1930.